

Quantitative understanding of the growth of Cu/Cu(001) including the determination of the Ehrlich-Schwoebel barrier at straight steps and kinks

Frits Rabbering, Herbert Wormeester, Frank Everts, and Bene Poelsema

MESA + Institute for Nanotechnology, University of Twente, P.O. Box 217, 7500 AE Enschede, The Netherlands

(Received 20 November 2008; published 2 February 2009)

The initial stages of homoepitaxial growth of Cu(001) have been studied by combining experiments and simulations. The investigated temperature window ranges from 200 to 300 K, the deposition rates vary from about 0.5 to 5 monolayer (ML)/min, and the coverage ranges up to about 10 ML. The simulated data have been extracted from a kinematic Monte Carlo approach using a bulk-continued fcc lattice and energetic activation barriers taken from recent literature. The experimental data are thermal energy helium-uptake curves measured *in situ* during growth. The Ehrlich-Schwoebel barriers for descent from $\langle 110 \rangle$ -oriented and $\langle 100 \rangle$ -oriented steps have been used as fitting parameters for the heights of the first and second maxima of the temporal oscillations in the He-uptake curves. Remarkable agreement has been achieved in the entire parameter space except for temperatures below about 230 K. The deviations in the latter range are attributed to failure of the bulk-continued fcc lattice due to, e.g., contraction, etc., becoming of importance for small adatom islands. This result allows an unequivocal determination of the Ehrlich-Schwoebel barrier associated with interlayer mass transport via a kink site (i.e., a $\langle 100 \rangle$ segment) in otherwise straight $\langle 110 \rangle$ steps, amounting to $E_{ES}^{(100)} = -5 \pm 3$ meV. The Ehrlich-Schwoebel barrier associated with $\langle 110 \rangle$ is determined at $E_{ES}^{(110)} = 120$ meV or higher. The perfect agreement between simulated and the experimental data in the wide range of parameter space also permits a quantitative evaluation of both coarsening, i.e., the increase in the lateral length scale of the structures and the kinetic roughening during growth. The lateral length scale varies with time to the power $n = 0.22 \pm 0.01$ in perfect agreement with experimental literature data. Roughening exponents $\beta = 0.5$ and 0.25 have been obtained for 250 and 290 K, respectively, also in very good agreement with previous experimental findings.

DOI: [10.1103/PhysRevB.79.075402](https://doi.org/10.1103/PhysRevB.79.075402)

PACS number(s): 68.55.A-, 68.49.Bc, 68.47.De, 81.15.Aa

I. INTRODUCTION

In crystal growth a variety of diffusion processes on surfaces are at the basis of various kinetic growth modes and morphology of the growth front. Homoepitaxial growth provides an excellent playground in which to study the relation between elementary diffusion processes and their collective outcome. The deposition of the same material assures the development of largely strain-free adlayers or multilayer films and avoids the complications arising from alloying. Even in the case of homoepitaxial growth adatom (or vacancy) structures may result in strain effects with electronic consequences.¹⁻⁴ Although there is some experimental evidence for strain in homoepitaxial systems,^{5,6} these effects are quite minor at not too low temperatures, still allowing monomer mobility. Therefore, we neglect these features and consider the fcc lattice model, i.e., the atoms at or near the surface occupy bulk-continued lattice sites, as a realistic framework for modeling the growth dynamics. In this approximation the diffusion processes are modeled as attempts to move an atom from one position to a neighbor position with a rate depending on its local surroundings. Two specific types of activated diffusion processes have to be distinguished (see Fig. 1), intralayer and interlayer diffusion processes. These determine to a large extent the morphology of the growing film (growth front). We roughly distinguish three kinds of growth modes: rough or multilayer growth, smooth or layer-by-layer growth, and, as an extreme representation of the latter, step flow growth. Precise knowledge of the rates of the various diffusion processes is required to understand the observed growth behavior at a specific temperature and deposition flux.

Only a few very elementary diffusion barriers are accessible for direct experimental observation. The barriers for most diffusion processes are obtained from calculations that consider the minimum energy path of a diffusion process. The diffusion barrier is found from the difference between the highest energy along this path with respect to the initial energy. Breeman *et al.*^{7,8} performed calculations on a few elementary processes. This was followed by Furman and co-workers,^{9,10} who used this method to produce a complete set of intralayer diffusion barriers for Cu on Cu(001) and other similar surfaces. A value of 0.48 eV was evaluated for the activation barrier of adatom diffusion over a terrace, while a value of 0.89 eV is found for detachment of a straight step edge, while diffusion along a step has a barrier of only 0.24 eV. This set of barriers was used in a kinetic Monte Carlo (kMC) simulation of the diffusion and deposition processes. They obtained a good correspondence between these simulations and the island shape and density in the early stages of submonolayer growth as observed in experiments over a wide range of temperature and flux. Long-range jumps as reported on Pt(110) (Ref. 11) may in principle exist on Cu(001) too. However, such events are not to be expected for the (low) temperature range considered here.

Since the experimental work of Ehrlich¹² and the theoretical work of Schwobel¹³ the diffusion process across a step edge is known to differ from diffusion on a terrace. Such interlayer diffusion processes are usually characterized by an additional barrier, the Ehrlich-Schwoebel (ES) barrier, added to the activation energy for diffusion on a terrace; see Fig. 1. Usually this barrier is positive and typically of the order of 60 meV (Refs. 14 and 15) for (001) terraces up to a value of

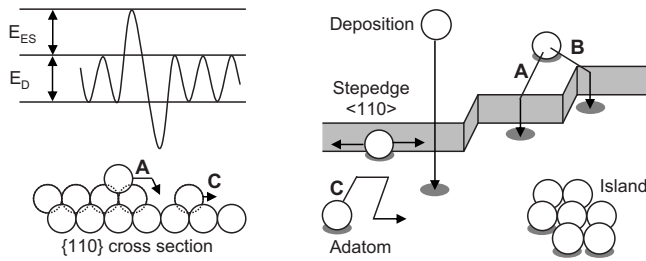


FIG. 1. Schematic picture of diffusion processes on a surface. The image on the right shows next to adatom and step-edge diffusion also the two relevant interlayer diffusion pathways: (A) via the close-packed step edge or (B) via kinks. The bottom left image depicts the situation near a step edge. The top left image shows the potential surface near this step edge, where E_{dif} represents the activation barrier for the intralayer diffusion of an adatom and E_{ES} represents the extra Ehrlich-Schwoebel barrier for interlayer diffusion.

a few hundred meV for close-packed terraces. It has been noted that the ES barrier may be negative, implying that descent across the step may require less thermal activation than migration back onto the terrace.¹⁴

The interlayer mass transfer processes are crucial in the balance between rough and layer-by-layer growths. Without mass transfer between terraces, a rough growth front develops with a characteristic lateral length scale set by the intralayer processes during very early stages of growth. Only if this length scale is similar to or larger than the step-step distance determined by the (local) vicinity of the surface, an extremely smooth growth front can develop, i.e., the growth proceeds by step flow. The homoepitaxial growth on Cu(001) is known to show all three kinetic growth modes depending on the deposition temperature and deposition rate; see Ref. 16 and references therein.^{17–21} This implies that temperature-dependent paths for interlayer mass transport are available. Two of these (see Fig. 1) are the transport across the thermodynamically favored straight $\langle 110 \rangle$ step edge, as well as across the $\langle 100 \rangle$ step edge. The latter is also associated with diffusion processes across kink sites in a $\langle 110 \rangle$ step edge. The relative importance of these two processes depends both on the energy barrier for diffusion and on the abundance of the actual pathways. The latter implies that the shape of adatom islands, i.e., the relative presence of $\langle 100 \rangle$ step edges, also influences the growth dynamics. The influence of this shape was used first to explain the re-entrant layer-by-layer homoepitaxial growth on Pt(111).²² The combination of these factors leads to complex interlayer mass transport in which the barrier for diffusion itself is not the only relevant parameter. It is well known that interlayer diffusion through a kink site, i.e., a $\langle 100 \rangle$ step segment, may involve different atomic processes. Conventionally the diffusion across the step was pictured as “rolling over,” in which the adatom ends as the new kink atom. However, the descending adatom may alternatively push out the original kink atom (C in the left-hand-bottom cartoon of Fig. 1). For certain configurations the resulting activation barrier for the latter is the lower one.²³ We explicitly note that the end results for the push-out and conventional events are indistinguishable in the homoepitaxial case considered here. Therefore,

we will further disregard these details. This implies that the obtained value for the Ehrlich-Schwoebel barrier will apply for the energetically cheapest process.

In their scanning tunnel microscope (STM) study of the decay of a large three-dimensional (3D) island with predominantly $\langle 110 \rangle$ steps, Li *et al.*²⁴ showed that on the Cu(001) surface the kinks in the $\langle 110 \rangle$ steps are the preferred sites for interlayer mass transport. This selective side descent mechanism occurs on a surface on which at least two different paths for interlayer diffusion are present, the straight $\langle 110 \rangle$ step edge and the kinks in this step. However, the latter pathway is associated with a much lower ES barrier than the first one. The theoretical study of Trushin *et al.*¹⁴ showed a similar difference. An ES barrier of 60 meV was evaluated for diffusion across the close-packed $\langle 110 \rangle$ step, while a negative barrier of -160 meV was obtained for diffusion paths across a kink site. This negative barrier implies that the presence of kinks facilitates the interlayer mass transport. The difference in mass transport across the $\langle 110 \rangle$ and $\langle 100 \rangle$ step edges was also found to explain the orientation of the etch-pit structures on Cu(001).²⁵ A similar etching behavior was previously found for Ag(001) by Teichert *et al.*²⁶ The ES barriers on the Ag(001) surface were also evaluated with molecular-dynamic simulations also providing a negative ES barrier for kink sites.²⁷ Alternatively, the ES barrier of the close-packed step edge was determined by comparing kMC simulations and the experimental film width (roughness) as obtained with STM.²⁸ With the assumption that the ES barrier of a kink site is zero, an ES barrier of the close-packed step edge of 70 ± 10 meV (Ref. 28) was found for Ag(001). This value was verified with a different experimental approach in which the amount of material in the second layer after deposition of 1 monolayer (ML) was used.²⁹

The reported energy values for the different interlayer transport paths agree qualitatively, all exhibiting that diffusion via kinks is easier than via steps. Quantitatively, the results differ significantly even to an extent that they give rise to different growth modes. Simulations with the lowest values of the ES barriers reported result in smooth layer-by-layer growth at $T=250$ K for homoepitaxial growth of Cu(001), while the highest values give rise to a rough growth front. A precise determination of these barriers is mandatory to understand multilayer growth. Experimentally the evolution of the growth front is easily measured with an *in situ* diffraction technique as it provides directly a measure of the surface roughness. Thermal energy atom scattering (TEAS) probes only the very surface and is in this case the best choice. Around 250 K, Poelsema *et al.*^{21,30} showed that in an out-of-phase condition, the specular reflected peak height shows oscillations with several maxima and minima. A gradual turnover from layer-by-layer growth toward rough growth was found. The developed film roughness depends on the temperature and deposited amount of material. In this paper we will compare the growth front evolution recorded experimentally with detailed simulations. In these simulations both the ES barriers across the close-packed $\langle 110 \rangle$ and the open $\langle 100 \rangle$ step edges are varied. This approach offers a powerful way to set a quantitative window for both barriers.

II. EXPERIMENTAL SETUP AND SIMULATION DETAILS

All experiments were performed in an UHV setup with a base pressure $<10^{-10}$ mbar. The sample was cleaned by sputter anneal cycles using 800 eV Ar ions and annealing at a temperature of 750 K. This resulted in an impurity level below the Auger electron spectroscopy (AES) detection limit. Further cleaning was checked with high-resolution low-energy electron diffraction (HR-LEED), which ultimately showed an average terrace length above 100 nm.^{5,6,21,31–33} The homoepitaxial growth experiments were monitored *in situ* with TEAS.^{21,30} A thoroughly desulfurized thermal evaporation Cu source was used. The TEAS system has a transfer width of about 25 nm, and contamination by the He beam was minimized by using 6.0 He that was further purified by a liquid nitrogen trap. Under these conditions the contamination level remained below the detection limit of AES.

The presence of thermally activated diffusion paths on the Cu(001) surface allows the simulation of the growth with a lattice model in the kMC scheme. The growth is simulated on an fcc substrate with 512×512 lattice sites per Cu(001) layer and periodic boundary conditions. For a given morphology, the rates of all diffusion pathways are added to the deposition rate and a random number generator determines whether a deposition process or a given diffusion process is performed. At a specific temperature the rates of the diffusion processes are determined by their activation barrier assuming a fixed frequency factor of 10^{13} s^{-1} . For intralayer diffusion processes Biham *et al.*⁹ evaluated the activation barriers by comparing experimental results with kMC simulations. Their tabulated activation energies on Cu(001) depend on the presence of the nearest-neighbor and next-nearest-neighbor atoms in the same layer. Due to symmetry, a set of 72 independent energy barriers was obtained. To allow multilayer growth two interlayer diffusion barriers are added to the simulation. These two diffusion paths describe the likelihood of mass transport “across” the $\langle 100 \rangle$ and $\langle 110 \rangle$ step edges. An additional barrier is introduced for both pathways, simulating the presence of an Ehrlich-Schwoebel barrier. Kink sites frequently present in the energetically favored $\langle 110 \rangle$ step edge are treated as $\langle 100 \rangle$ microfacets. To prevent overhangs, an immediate downfunneling process is incorporated.³⁴

This simulation scheme is already quite demanding for submonolayer growth at a relevant temperature of 250 K.⁹ At this temperature interlayer transport is significant, i.e., the growth front gets smoother, which can be concluded already directly from the presence of the first and second maxima in He specular reflectivity oscillations.^{17,20,21} It is thus important to be able to simulate at this temperature and a few tens of kelvins higher. At these higher temperatures, most of the simulation time is spent on fast processes that do not alter surface morphology such as step-edge diffusion. The result of this fast diffusion process is that the atom attached to the step edge will after some time be more strongly bonded in one or more possible end positions. This step-edge diffusion process is so fast that it does not influence any of the other processes but does require a major part of the CPU time. It can be slowed down without consequences for the growth

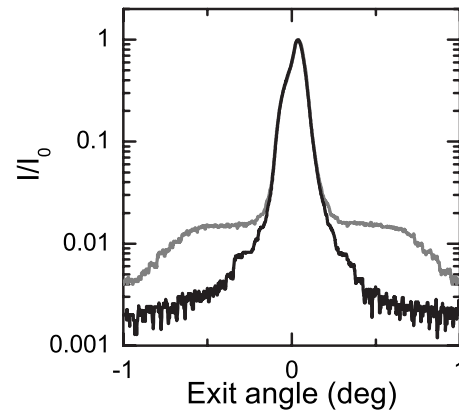


FIG. 2. Normalized He-specular beam profiles of the initially smooth Cu(001) surface (black curve) and after deposition of 1 ML at 270 K (gray curve). The profiles have been measured at an out-of-phase condition. The exit angle indicated is relative to the out-of-phase condition. The peak shape reveals some mosaicity ($<0.05^\circ$) of the substrate within the illuminated spot.

morphology as long as the probability of the various end positions is not altered. Therefore, we follow Biham *et al.*,⁹ who incorporated an artificial suppression of paths with an energy barrier below 400 meV to suppress spending too much time on these fast processes. The activation energy for diffusion, E , of these paths is artificially increased with a factor of $\alpha(400 \text{ meV} - E)$. After careful evaluation of the influence of the morphology, a value of $\alpha=0.6$ was found to suffice. However, the process of vacancy creation at a kink site had to be reduced additionally to suppress the otherwise noticeable influence of vacancy diffusion on the island shape.

III. EXPERIMENTAL RESULTS

The intensity change of a He atom specular reflected beam has been used in several studies of the homoepitaxial growth of Cu(001).^{18,20,31,35–37} The temporal evolution of the height of the He specular beam under out-of-phase conditions during deposition is a sensitive monitor of the development of the roughness of the growth front. In these experiments, it was assumed that the height is proportional to the integrated central spike whose strength is determined by the constructive interference of He atoms scattered from the terraces on the surface. The validity of this assumption has been checked with the experiment shown in Fig. 2. It shows the profile of the specular beam for the pristine surface and after deposition of 1 ML at 270 K. Both profiles are normalized to the maximum intensity recorded. The profile of the central spike recorded after 1 ML deposition is indeed very similar to that of the clean surface. The similarity implies that the height of the specular He beam can indeed be used as a measure of the integrated central spike.

The normalized height, I/I_0 , of the specular reflected He beam under an out-of-phase condition depends on the balance between the surface integrated fractional areas of the exposed odd and even layers. If we disregard the influence of diffuse scattering from point or line defects this intensity is

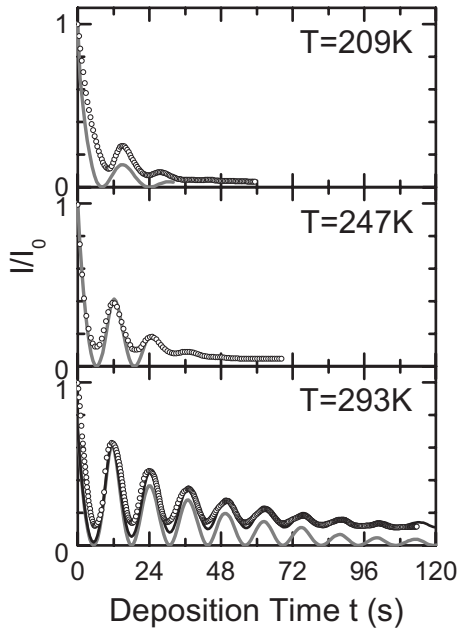


FIG. 3. Temporal evolution of the normalized specular He peak height, I/I_0 , during homoepitaxial growth of Cu(001) at substrate temperatures of 209, 247, and 293 K (O) and the result of simulations (gray line). For 293 K the simulation result corrected for the finite instrumental resolution is also shown (black solid line); see text.

normalized to the intensity of the initially smooth surface I_0 ,

$$\frac{I}{I_0} = \left[\sum_{i=\text{even}} (\theta_i) - \sum_{i=\text{odd}} (\theta_i) \right]^2, \quad (1)$$

with $\sum_i (\theta_i) = 1$. Figure 3 shows some representative variations in the height of the specularly reflected He peak during deposition in the studied temperature range. The deposition rate amounts to about 5 ML/min. The presence of a maximum is a sensitive probe of the layer distribution, i.e., basically layer-by-layer growth. The temporal oscillations reveal damped layer-by-layer growth. Around room temperature up to nine oscillations can be observed indicating a pronounced layer-by-layer growth mode. The interlayer mass transport is substantially reduced at 247 K, resulting in only a few oscillations. At low temperature (209 K) only two small maxima can be discerned. The low value of the first maximum indicates that already substantial nucleation of adatom islands in the second layer has occurred before completion of the first layer. If one makes the reasonable assumption that around monolayer completion (i.e., around the first and second maxima) one is dealing with effectively a three exposed layers system, we can determine the layer distribution of deposited material. At the first maximum the amount of material in the second layer follows from the deficit of the normalized specular He-peak height by

$$\theta_2 = \frac{1}{4} \left(1 - \sqrt{\frac{I}{I_0}} \right). \quad (2)$$

The amount of material in the second layer is thus only about 9% at 247 K and 5% at 293 K, illustrating the high sensitivity of this method on surface roughness.

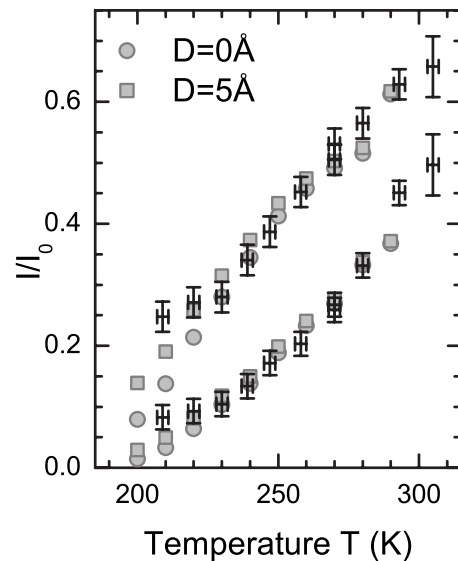


FIG. 4. Intensities of the first and second maxima in the He reflectance curve as a function of temperature (+). The values are all normalized to their respective values for the smooth surface at the corresponding temperature. Results from simulations of the specular He reflectance are shown. The influence of diffuse scattering by step edges is depicted by the simulation results without diffuse scattering (\square) and with a 5-Å-wide zone along the step edge regarded to contribute to diffuse scattering (O); see text.

The values of the first and second intensity maxima were used as a measure of the initial roughening of the interface. For the temperature range of 210–310 K the height of these maxima is depicted in Fig. 4. Above 230 K the growth proceeds in an ever smoother way with increasing temperature. Below 230 K much less temperature dependence is observed, indicating that the roughness of the surface after 1 ML deposition does not depend strongly on temperature in this range. This indicates a reduced activity of diffusion processes on the surface.

IV. SIMULATION RESULTS

The validity of the simulation results was tested first by evaluating the average island separation L for 0.5 ML coverage. This characteristic length can be obtained experimentally as a function of temperature after deposition of 0.5 ML with HR-LEED measurements from the radius of the diffraction ring.^{31,38} The measured average island separation is shown in Fig. 5 as well as those obtained from the simulations. The calculated values were obtained from the ring position in diffraction images evaluated for the simulated morphologies. This provides a common base for the length scale determination. The similarity between experimental data points and simulations is convincing and certainly within statistical error margins. Figure 5 also shows a solid line that depicts the relation between the island separation L and temperature T based on nucleation theory.^{39,40} The adatom diffusion energy, i.e., 0.48 eV, and the assumption that a dimer is a stable nucleus provide the slope of the shown curve. The offset is chosen to give the best fit. Although the simulation

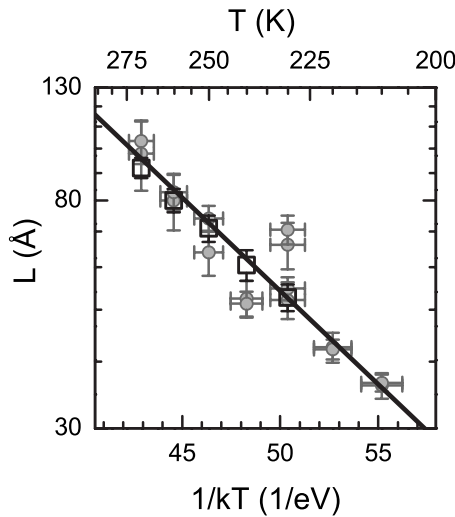


FIG. 5. Average island separation L after 0.5 ML deposition versus substrate temperature evaluated from HR-LEED experiments (●) and from diffraction patterns of the simulated morphologies (□). The solid line indicates the distance-temperature dependence predicted by rate equations based on the adatom diffusion energy and assuming a dimer as stable nucleus (Ref. 39).

contains a manifold of diffusion processes, the adatom diffusion plays apparently the dominant role in the determination of the L - T dependence as expected.

The morphology evolution as a function of both the ES barriers for the straight step and at kinks was simulated. These simulated morphologies were compared with experimental observations by calculating the height of an out-of-phase specularly reflected He beam. Figure 6 shows the dependence of the normalized out-of-phase height of the specular He peak on the straight step and kink site ES barriers on the intensity after the deposition of 1 ML at 270 K. A low He reflectivity is found for a combination of high ES barriers for both step-edge sites, leading to rough growth fronts. Low ES barriers result in only a small amount of

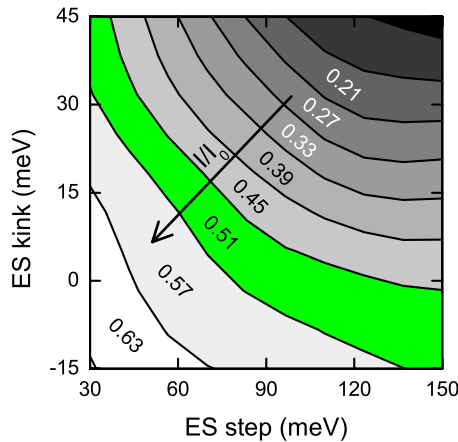


FIG. 6. (Color online) Calculated normalized He specular peak height at the first maximum as a function of the two ES barriers after deposition of 1 ML at $T=270$ K. The green area indicates the region that provides an intensity similar to the experimental value of 0.51.

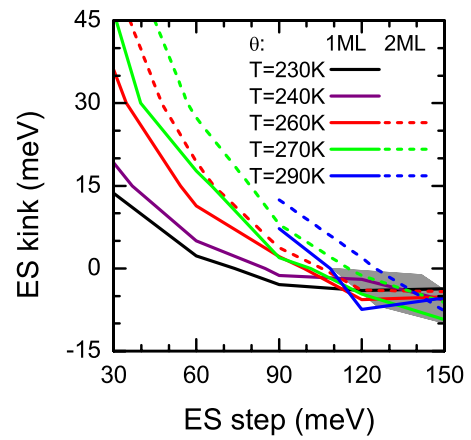


FIG. 7. (Color online) Combinations of the two ES barriers that provide the measured specularly reflected He intensity after 1 or 2 ML deposition at temperatures of 230, 240, 260, 270, and 290 K. The shaded area indicates the region of overlap of these curves taking into account the experimental and simulation accuracies.

material in the second layer at the position of the first maximum in the oscillations. Experimentally a normalized He-specular peak height of 0.51 ± 0.03 was found for this temperature (see Fig. 4). This intensity could be reproduced in the simulation by a nonunique combination of the ES barrier at straight steps and ES barrier at kink sites as indicated by the green band. The width of the intensity areas in Fig. 6 reflect the combined accuracy of experiments and simulations. The influence of the two ES barriers on the roughening of the surface depends on the substrate temperature. Therefore, a different combination of the two barriers that provide the experimentally observed intensity is obtained for another temperature. Figure 7 shows the ES barrier window that gives rise to unique agreement between the calculated and measured normalized heights of the specular He peak at the first maximum in the peak height oscillations obtained at 230, 240, 260, 270, and 290 K. Also included, denoted with the dashed curves, are the results for the comparison of the simulated and measured intensity at the second maximum in the intensity oscillations for deposition at 260, 270, and 290K. This combination of simulations and experimental observations allows us to determine a narrow window of allowable ES barriers for descent via kink sites and a lower estimate for the ES barrier for crossing straight $\langle 110 \rangle$ steps. The barrier for the kink site or $\langle 100 \rangle$ step is determined at $E_{ES\langle 100 \rangle} = -5 \pm 3$ meV, i.e., the barrier is slightly negative. The error margin for the kink barrier is quite small as a small change in its value has a large influence on the amount of interlayer mass transport. For the close-packed $\langle 110 \rangle$ step a lower limit of $E_{ES\langle 110 \rangle} = 120$ meV is found. The value determined for this step-edge barrier has a much larger uncertainty. The upper limit is actually inaccessible at present. Note that under the conditions considered here interlayer diffusion proceeds almost exclusively via kink sites. Mass transport across the $\langle 110 \rangle$ step edges is significant only for temperatures well above 290 K. However, this temperature range is at this moment too challenging for computational efforts.

TEAS is very sensitive to disorder on the surface, and diffuse scattering from step edges attenuates the actual inten-

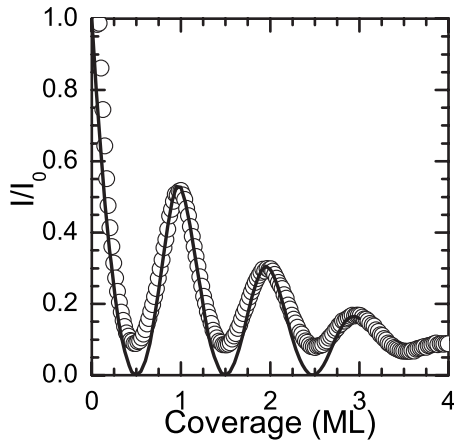


FIG. 8. Cu-uptake curve, i.e., the normalized He specular peak height for Cu(001) as a function of time during deposition at a rate of 0.5 ML/min and at 250 K. Both experimental points (\circ) and simulation results (solid line) are shown.

sity of the specular reflected He beam.^{41,42} For Pt(111), a diffuse scattering zone with a width of ≈ 10 Å around the step edge was determined.^{43–45} These Pt step edges show a particularly high Debye moment^{46,47} and are expected to show much larger diffuse scattering than step edges on a Cu(001) surface. Therefore, a value of 5 Å for the width of the diffuse scattering zone is much more appropriate than the rough estimate of 13 Å by Sanchez *et al.*⁴² This value was used to evaluate the simulated intensity oscillations by neglecting the contributions from a zone around the step edges. Figure 4 shows the influence of diffuse scattering from step edges, and we found that a 5 Å wide zone gives results similar to a vanishing diffuse scattering zone. The values found for the ES barriers are thus not influenced by this effect.

Temporal He-intensity oscillations at various temperatures were evaluated with the determined barriers and are compared to the experimental results in Fig. 3. The simulated curves show much more pronounced minima as a result of the fact that the transfer width of the instrument is neglected in Eq. (1). This shortcoming is more prominent for higher temperatures. This can be mended by a convolution of the simulated He diffraction pattern with a Gaussian broadening function with a full width at half maximum (FWHM) of 1% of the Brillouin zone. This provides a He growth-oscillation curve that is highly similar to the experimentally recorded one. Note that the intensity of the first maximum is hardly affected by this correction. It is, therefore, not necessary to correct the simulated data for this effect for the derivation of the ES barrier.

All experiments and simulations shown so far were performed at a deposition rate of 5 ML/min. Figure 8 shows a growth experiment and a simulation at 250 K but at about ten times reduced flux of 0.5 ML/min. A larger number of oscillations are observed at this growth rate. Also at this much reduced rate, the simulations reproduce this measurement with remarkable accuracy, providing solid faith in their validity in the considered parameter space.

V. COARSENING AND INTERFACE ROUGHENING IN MULTILAYER GROWTH

The evolution of the local interface height in multilayer growth has been described with continuum theory. Standard ingredients for such an approach are a statistical fluctuation of the deposition flux across the surface and diffusion and coarsening mechanisms.^{48,49} Dynamical exponents are used to characterize the temporal evolution of the growth. Siegert and Plischke⁵⁰ showed that the first of the three dynamical exponents describes the shape of the islands. This exponent equals one for molecular-beam epitaxy (MBE) growth with slope selection. This also applies for Cu homoepitaxial growth at normal incidence. The two other dynamical exponents describe the evolution of the interface roughness and the change in characteristic length scale with coverage. The evolution of the length scale was studied experimentally for Cu(001) homoepitaxy by Wendelken and co-workers^{10,38,51} at a temperature of 299 K. They reported a relation between the separation between mounds, L , and coverage θ according to $L \propto \theta^n$, with $n \approx 0.23$ from STM measurements for a coverage up to 100 ML. Figure 9(a) shows the change in average distance between mounds L for the present simulation results. This distance was determined from the position of the minimum in the autocorrelation function of a surface morphology r_0 as $L = 2r_0$. All simulations in the range of 200–290 K show a similar value of $n = 0.22 \pm 0.01$, in good agreement with the experimental value at 299 K. The temperature-independent relative change in L with coverage implies that also after the deposition of 10 ML the average distance between mounds shows the same temperature dependence as adatom islands in submonolayer coverage. This is illustrated in Fig. 9(b) which shows the relation between the average mound distance and temperature for 10 ML. Note that the latter is quite similar to Fig. 5, but in the present figure the distance was determined from the autocorrelation of morphology images. The temperature dependence of the average mound separation at 10 ML can still be described by submonolayer nucleation theory with the activation barrier of an adatom and assuming the dimer as the stable nucleus. This behavior was already found experimentally on Cu(001) for a smaller coverage window by evaluating the temperature-dependent mound separation after deposition of 15 and 20 ML.^{21,31} Similar behavior has also been reported for Fe/Fe(001) (Ref. 52) and Ag/Ag(001).²⁸

The third dynamic exponent describes the relation between the root-mean-square (rms) roughness w and coverage, $w \propto \theta^\beta$. This exponent has been measured by several groups^{37,53} for Cu on Cu(001). Of special interest is the decrease in this parameter with decreasing temperature below 200 K.³⁷ A re-entrant smooth growth for low temperatures was suggested as an explanation as was first observed for Pt(111).²² The correspondence between TEAS data and the simulations presented allows us to use the latter with confidence to explore the temperature dependence of the roughness evolution and thus of the exponent β . Figure 10(a) shows the change in roughness with coverage in a temperature range of 200–290 K. Already at 215 K a few oscillations in the rms can be observed. A quite good initial layer-by-layer growth is especially present at high temperatures. A

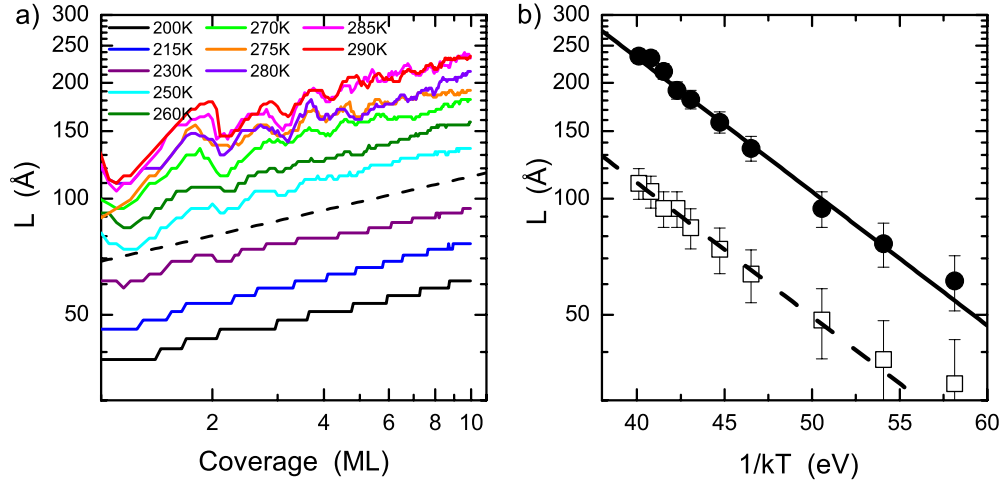


FIG. 9. (Color online) (a) Change in average distance between mounds L as a function of coverage for temperatures in the range of 200–290 K. The distance L is determined as twice the distance of the minimum in the autocorrelation function of the morphology. The dashed line indicates the relation $L \propto \theta^{0.22}$. (b) Average distance L at 10 (●) and 0.5 ML (□) as a function of temperature. The lines indicate the temperature dependence expected from rate equation analysis (cf. Fig. 5). These lines are fitted to L at 10 ML (solid line) and 0.5 ML (dashed line).

very different increase in roughness with coverage is observed for the various temperatures. The largest relative increase in the roughness is observed for temperatures in the range of (≈ 5 –10 ML) 250–275 K. The roughening exponent β is derived from the high coverage range in this graph and represents the value of this exponent in this coverage range. The value of this exponent can change with coverage and for Ag/Ag(001) a very different value below and above a coverage of 100 ML is found.⁵⁴ The temperature dependence of β for the presented simulations is shown in Fig. 10(b). An increase in β with temperature is observed between 200 and 250 K, while a steep decrease in β with temperature is observed from 280 to 290 K. The value of β at 250 K is consistent with the experimental observation from x-ray diffraction.⁵³ These authors noted a decrease to a value of 0.33 at 290 K, i.e., a more gradual decrease in β with increasing temperature is observed experimentally. The difference is probably the result of the experimental polar angle of

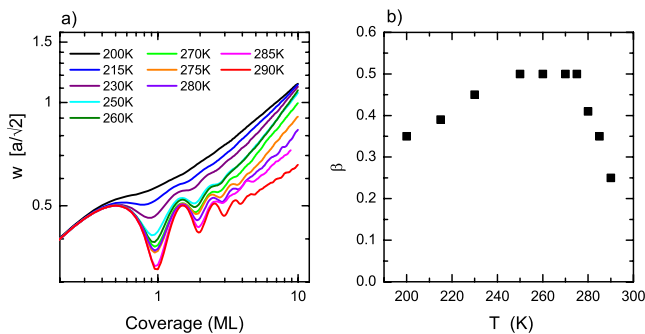


FIG. 10. (Color online) (a) Increase in the rms w with coverage in the temperature range of 200–290 K. The rms is normalized to the interlayer distance $a/\sqrt{2}$, with $a=2.55$ Å as the nearest-neighbor distance for Cu. (b) The value of the dynamic roughness exponent β as a function of temperature.

deposition of around 60° .⁵⁵ The lower value of β at 200 K differs from the experimental values of 0.5 (Refs. 37 and 53) at this temperature. We already noted deviations between TEAS results and simulations at this temperature (see Fig. 4) that suggest the presence of additional diffusion pathways relevant at low temperature.

VI. DISCUSSION

The detailed comparison of the experimental and simulated growth oscillation curves allows us to pinpoint both the ES barriers of the straight step edge and kink sites. The obtained values show that the kink's position (almost) exclusively facilitates the interlayer diffusion process in the temperature range of 230–290 K. This is consistent with a similar observation made for ion-induced surface morphologies.²⁵ STM measurements of island decay also showed a selective site descent mechanism that favors kinks as the pathway for interlayer diffusion.²⁴ However, the latter authors used substantially higher values for the ES barriers, with 90 meV for the barrier at kink sites. We emphasize that such a value would result in a very rough growth up to room temperature, contradicting the TEAS measurements. Li *et al.*²⁴ used a difference between the two ES barriers of 100 meV. The present study finds a minimum barrier difference of 120 meV. Note that a doubling of the kink density would result in an increase in the barrier for kink sites of only 15 meV. We believe that the kink density obtained in the simulations is well within this margin.

An effective ES barrier of 125 meV was experimentally evaluated in a temperature range of 360–400 K by Gerlach *et al.*⁵⁶ These experimental conditions are far outside our present range. The value of the effective barrier is very similar to the lower limit of the $\langle 110 \rangle$ step-edge barrier found in this work. It is quite conceivable that in this higher-

temperature range the interlayer mass transport takes place predominantly across the $\langle 110 \rangle$ step edge. The number of kink sites will be extremely small, and at 400 K the probability for descent across a kink site has become only about 40 times more probable than interlayer diffusion across the straight step edge. (At 300 K this ratio is still 150 times.) Accordingly, a rough estimate then leads to the conclusion that kink concentrations of less than 1% are completely consistent with our results. Considering the huge adatom structures in the low energy electron microscopy (LEEM) study of Gerlach *et al.*,⁵⁶ this is a very likely situation.

Below 230 K (see Fig. 4), the simulations show a rougher growth front than those experimentally observed. A change in growth mode at this temperature was expected from the work of Dürr *et al.*⁵¹ They found that below 223 K the variation in the average distance between adatom islands with temperature was different, i.e., its variation is smaller than that above this temperature. A smoother growth front at lower temperatures has also been reported by many authors (e.g., Refs. 53, 55, and 57). At these low temperatures, transient mobility has been suggested to provide an additional pathway for interlayer mass transport). However, molecular-dynamics simulations with an embedded atom potential (EAM) did not show clear evidence of such an effect.⁵⁸ We do stress that transient mobility confined to one hop cannot be excluded and would fully account for the observed deviations between experiments and simulations. Several effects are potential candidates to explain this behavior. First, the kink rounding effect was used to explain results on Ag(001) as it leads to a higher densities of kinks.^{15,54} The kink rounding effect was also recently used in a simulation to explain the observed growth behavior at low temperatures.⁵⁹ A second effect to consider is the collective effects of clusters of adatoms on the upper terrace near a step edge. Teichert²⁶ already showed in calculations that such clusters of a few atoms near a kink position yields a reduced ES barrier on Ag(001) compared to the ES barrier for the kink site. This would lead to a slightly smoother growth front for temperatures just below the onset of adatom diffusion. It has also been reported that ES barriers may be reduced on smaller adatom islands.²⁶ Calculations also show that small islands show a contraction.^{1,3} On top of the contracted islands the activation energy for diffusion is lower and therefore the attempt frequency for descent increases.⁶⁰ This would inevitably lead to enhanced interlayer diffusion. All these effects, individually or combined, give rise to smoother growth fronts. Our simulations do not take these effects in account, which limits their use to a temperature of 230 K and above.

We emphasize that admittedly the simulation of growth is a highly complex enterprise in which a multitude of thermally activated processes may be relevant. The activation barriers for these processes have to be determined quite accurately and where possible, individually in order to reliably describe growth. The problem is further complicated by highly entangled processes and their complex interplay with respect to the evolving morphology. Especially dealing with processes with inherently very widely varying rates is definitely hazardous and requires intense attention. Being well aware of a variety of possible pitfalls we have scrutinized

internal consistency of our simulated results. With initial surprise and since then ever-growing confidence, we have performed a large number of comparisons between simulated results and experiments. We stress that with one set of parameters, combining calculated ones with the experimentally determined values for the ES barriers associated with straight $\langle 110 \rangle$ steps and ($\langle 100 \rangle$ microfaceted) kink sites, we are able to uniquely describe and understand experimental data quantitatively. This holds for a relatively wide temperature range (230–290 K), in which relevant diffusion rates, e.g., for monomer diffusion varied by 2 orders of magnitude or more, deposition rates varying by an order of magnitude and, above all, a wide variation in film thicknesses from 0.5 up to 20 ML. Especially the latter provides a very sensitive benchmark because of the cumulative nature of consequence of failing descriptions would lead to strong deviations of layer distributions, adatom sizes, and kink concentrations. The quality of our quantitative description provides a great deal of confidence in the global correctness of the simulations, at least for all relevant processes active in the investigated parameter space.

The evolution of the morphology of Cu(001) homoepitaxy was studied by several groups employing both various diffraction techniques and STM. These techniques all provide a different view on this morphology evolution. The specular He reflection (TEAS) data in this work at the highest temperature are quite similar to the ones recorded by Miguel *et al.*¹⁸ for temperatures of 318 K and above. Ernst *et al.*²⁰ published TEAS data in the range considered in this work that suggest a slightly smoother growth at 250 K. This smoother growth is in line with the larger distance between islands at 0.5 ML measured by this group³⁶ and suggests a minor calibration issue on the temperature scale.

VII. CONCLUSION

The interface roughening during the homoepitaxial growth of Cu(001) has been monitored with TEAS in the temperature range of 200–300 K. The normalized height of the specularly reflected He peak in the first maxima of the growth oscillation curves provides a data set that allows the determination of the Ehrlich-Schwoebel barriers of the $\langle 100 \rangle$ step edge and estimate a lower limit for the $\langle 110 \rangle$ step edge. This determination is performed by comparing the experimental growth front roughening with simulations. Only for an ES barrier of 120 meV (or more) for the straight $\langle 110 \rangle$ step edge and -5 meV for the kink $\langle 100 \rangle$ step edge the simulations lead to agreement with the experimental results. The barrier for the straight step edge is a lower limit and reflects the fact that under the investigated conditions the interlayer mass transport occurs predominantly via the kink sites. The nine maxima of the specularly reflected He intensity recorded at 290 K are reproduced well by the simulation scheme if the experimental broadening is taken into account. With these parameters we can describe quantitatively the morphology of thin films up to at least 9 ML in a temperature range of 230–290 K and for a deposition rate varying by an order of magnitude (0.5–5 ML/min.). The simulated interface roughness shows a scaling exponent with respect to the cov-

erage amounting to 0.5 at 250 K and 0.25 at 290 K, similar to previous experiments.⁵³ Concluding, the developed powerful kMC simulation reliably describes the morphology of the growing Cu(001) surface. We expect that it will do so also for other nonreconstructing metal (001) surfaces, such as Ag(001) and Ni(001).

ACKNOWLEDGMENTS

This work is part of the research programme of the Stichting Fundamenteel Onderzoek der Materie (FOM), which is financially supported by the Nederlandse Organisatie voor Wetenschappelijk Onderzoek (NWO).

- ¹O. V. Lysenko, V. S. Stepanyuk, W. Hergert, and J. Kirschner, *Phys. Rev. Lett.* **89**, 126102 (2002).
- ²D. Sander, S. Ouazi, V. Stepanyuk, D. Bazhanov, and J. Kirschner, *Surf. Sci.* **512**, 281 (2002).
- ³V. Stepanyuk, D. Tsvilin, D. Sander, W. Hergert, and J. Kirschner, *Thin Solid Films* **428**, 1 (2003).
- ⁴O. V. Lysenko, V. S. Stepanyuk, W. Hergert, and J. Kirschner, *Phys. Rev. B* **68**, 033409 (2003).
- ⁵M. Ovsyanko, G. Stoian, H. Wormeester, and B. Poelsema, *Phys. Rev. Lett.* **93**, 086103 (2004).
- ⁶M. M. Ovsyanko, Ph.D. thesis, University of Twente (2006).
- ⁷C. Lee, G. T. Barkema, M. Breeman, A. Pasquarelloc, and R. Car, *Surf. Sci.* **306**, L575 (1994).
- ⁸M. Breeman, G. T. Barkema, and D. O. Boerma, *Surf. Sci.* **323**, 71 (1995).
- ⁹O. Biham, I. Furman, M. Karimi, G. Vidali, R. Kennett, and H. Zeng, *Surf. Sci.* **400**, 29 (1998).
- ¹⁰I. Furman, O. Biham, J.-K. Zuo, A. K. Swan, and J. F. Wendelken, *Phys. Rev. B* **62**, R10649 (2000).
- ¹¹T. R. Linderoth, S. Horch, E. Lgsgaard, I. Stensgaard, and F. Besenbacher, *Phys. Rev. Lett.* **78**, 4978 (1997).
- ¹²G. Ehrlich and F. G. Hudda, *J. Chem. Phys.* **44**, 1039 (1966).
- ¹³R. L. Schwoebel, *J. Appl. Phys.* **40**, 614 (1969).
- ¹⁴O. S. Trushin, K. Kokko, P. T. Salo, W. Hergert, and M. Kotrla, *Phys. Rev. B* **56**, 12135 (1997).
- ¹⁵J. W. Evans, P. A. Theil, and M. C. Bartelt, *Surf. Sci. Rep.* **61**, 1 (2006).
- ¹⁶G. Rosenfeld, B. Poelsema, and G. Comsa, *Epitaxial Growth Modes Far from Equilibrium* (Elsevier, New York, 1997), Chap. 3.
- ¹⁷L. J. Gomez, S. Bourgeal, J. Ibanez, and M. Salmeron, *Phys. Rev. B* **31**, 2551 (1985).
- ¹⁸J. J. de Miguel, A. Sanchez, A. Cebollada, J. M. Gallego, J. Ferron, and S. Ferrer, *Surf. Sci.* **189–190**, 1062 (1987).
- ¹⁹J. Ferron, J. M. Gallego, A. Cebollada, J. J. De Miguel, and S. Ferrer, *Surf. Sci.* **211–212**, 797 (1989).
- ²⁰H.-J. Ernst, F. Fabre, and J. Lapujoulade, *Surf. Sci.* **275**, L682 (1992).
- ²¹L. C. Jorritsma, M. Bijnagte, G. Rosenfeld, and B. Poelsema, *Phys. Rev. Lett.* **78**, 911 (1997).
- ²²R. Kunkel, B. Poelsema, L. K. Verheij, and G. Comsa, *Phys. Rev. Lett.* **65**, 733 (1990).
- ²³G. Henkelman and H. Jónsson, *Phys. Rev. Lett.* **90**, 116101 (2003).
- ²⁴M. Z. Li, J. F. Wendelken, B. G. Liu, E. G. Wang, and Z. Zhang, *Phys. Rev. Lett.* **86**, 2345 (2001).
- ²⁵P. Broekmann, A. Mewe, H. Wormeester, and B. Poelsema, *Phys. Rev. Lett.* **89**, 146102 (2002).
- ²⁶C. Teichert, C. Ammer, and M. Klaua, *Phys. Status Solidi A* **146**, 223 (1994).
- ²⁷U. Kurpick and T. S. Rahman, *Phys. Rev. B* **57**, 2482 (1998).
- ²⁸K. J. Caspersen, C. R. Stoldt, A. R. Layson, M. C. Bartelt, P. A. Theil, and J. W. Evans, *Phys. Rev. B* **63**, 085401 (2001).
- ²⁹P. A. Thiel and J. W. Evans, *J. Phys. Chem. B* **108**, 14428 (2004).
- ³⁰P. Bedrossian, G. Poelsema, B. Rosenfeld, L. C. Jorritsma, N. N. Lipkin, and G. Comsa, *Surf. Sci.* **334**, 1 (1995).
- ³¹L. C. Jorritsma, Ph.D. thesis, University of Twente (1997).
- ³²S. van Dijken, L. C. Jorritsma, and B. Poelsema, *Phys. Rev. Lett.* **82**, 4038 (1999).
- ³³S. van Dijken, Ph.D. thesis, University of Twente (2000).
- ³⁴J. W. Evans, *Phys. Rev. B* **43**, 3897 (1991).
- ³⁵H.-J. Ernst, F. Fabre, and J. Lapujoulade, *Phys. Rev. Lett.* **69**, 458 (1992).
- ³⁶H.-J. Ernst, F. Fabre, and J. Lapujoulade, *Phys. Rev. B* **46**, 1929 (1992).
- ³⁷H.-J. Ernst, F. Fabre, R. Folkerts, and J. Lapujoulade, *Phys. Rev. Lett.* **72**, 112 (1994).
- ³⁸J. K. Zuo and J. F. Wendelken, *Phys. Rev. Lett.* **78**, 2791 (1997).
- ³⁹J. A. Venables, *Philos. Mag.* **27**, 697 (1973).
- ⁴⁰I. V. Markov, *Crystal Growth for Beginners* (World Scientific, Singapore, 1995).
- ⁴¹L. K. Verheij, B. Poelsema, and G. Comsa, *Surf. Sci.* **162**, 858 (1985).
- ⁴²A. Sanchez and S. Ferrera, *Surf. Sci.* **187**, L587 (1987).
- ⁴³B. Poelsema, S. T. de Zwart, and G. Comsa, *Phys. Rev. Lett.* **49**, 578 (1982).
- ⁴⁴B. Poelsema, S. T. de Zwart, and G. Comsa, *Phys. Rev. Lett.* **51**, 522 (1983).
- ⁴⁵B. Poelsema and G. Comsa, *Scattering of Thermal Energy Atoms for Disordered Surfaces*, Springer Tracts in Modern Physics Vol. 115 (Springer, New York, 1989).
- ⁴⁶K. Besocke, B. Krahl-Urban, and H. Wagner, *Surf. Sci.* **68**, 39 (1977).
- ⁴⁷J. Y. Park, G. M. Sacha, M. Enachescu, D. F. Ogletree, R. A. Ribeiro, P. C. Canfield, C. J. Jenks, P. A. Theil, J. J. Sáenz, and M. Salmeron, *Phys. Rev. Lett.* **95**, 136802 (2005).
- ⁴⁸A. L. Barabási and H. E. Stanley, *Fractal Concepts in Surface Growth* (Cambridge University Press, Cambridge, 1995).
- ⁴⁹Y. Zhao, G.-C. Wang, and T.-M. Lu, *Characterization of Amorphous and Crystalline Rough Surface: Principles and Applications*, Experimental Methods in Physical Sciences Vol. 37 (Academic, New York, 2001).
- ⁵⁰M. Siegert and M. Plischke, *Phys. Rev. Lett.* **73**, 1517 (1994).
- ⁵¹H. Dürr, J. F. Wendelken, and J. K. Zou, *Surf. Sci.* **328**, L527 (1995).
- ⁵²J. A. Stroscio, D. T. Pierce, M. D. Stiles, A. Zangwill, and L. M. Sander, *Phys. Rev. Lett.* **75**, 4246 (1995).

- ⁵³C. E. Botez, P. F. Miceli, and P. W. Stephens, *Phys. Rev. B* **64**, 125427 (2001).
- ⁵⁴K. J. Caspersen, A. R. Layson, C. R. Stoldt, V. Fournée, P. A. Theil, and J. W. Evans, *Phys. Rev. B* **65**, 193407 (2002).
- ⁵⁵V. Borovikov, Y. Shim, and J. G. Amar, *Phys. Rev. B* **76**, 241401(R) (2007).
- ⁵⁶R. Gerlach, T. Maroutian, L. Douillard, D. Martinotti, and H.-J. Ernst, *Surf. Sci.* **480**, 97 (2001).
- ⁵⁷H.-J. Ernst, F. Fabre, R. Folkerts, and J. Lapujoulade, *J. Vac. Sci. Technol. A* **12**, 1809 (1994).
- ⁵⁸F. Montalenti and A. F. Voter, *Phys. Rev. B* **64**, 081401(R) (2001).
- ⁵⁹Y. Shim and J. G. Amar, *Phys. Rev. B* **73**, 035423 (2006).
- ⁶⁰H. Brune, K. Bromann, H. Röder, K. Kern, J. Jacobsen, P. Stoltze, K. Jacobsen, and J. Nørskov, *Phys. Rev. B* **52**, R14380 (1995).